Received: 13 July 2021, Accepted: 16 August 2021, Published: 30 November 2021, Publisher: UTP Press, Creative Commons: CC BY-NC-ND 4.0

GLYCEROL-ASSISTED SOL-GEL SYNTHESIS OF NITROGEN-DOPED TITANIUM DIOXIDE FOR VISIBLE LIGHT-DRIVEN PHOTODEGRADATION OF INDOOR GASEOUS FORMALDEHYDE

Elyne Chng[1], Nurul Tasnim Sahrin[1,2*], Rab Nawaz[1,2], Chong Fai Kait[1,2], Siew Ling Lee[3,4]

[1]Fundamental and Applied Sciences Department, Universiti Teknologi PETRONAS, Malaysia
[2]Center of Innovative Nanostructures and Nanodevices, Institute of Autonomous System, Universiti Teknologi PETRONAS, Malaysia
[3]Center for Sustainable Nanomaterials, Ibnu Sina Institute for Scientific and Industrial Research, Universiti Teknologi Malaysia
[4]Chemistry Department, Faculty of Science, Universiti Teknologi Malaysia

*Email: nurul_17007753@utp.edu.my

ABSTRACT

In the present paper, the synthesis of nitrogen-doped titanium dioxide (N-doped TiO_2) photocatalyst and its application for photodegradation of gaseous formaldehyde are reported. The N-doped TiO_2 was synthesized via the glycerol-assisted sol-gel technique. The effect of various synthesis parameters such as nitrogen to titanium (N:Ti) molar ratio, calcination temperature, calcination duration and TiO_2 loading was investigated on the photocatalytic properties of TiO_2 and photodegradation of HCHO vapor. The characterization results obtained through different analytical techniques such as XRD, XPS, FESEM, DRUV-Vis, and BET revealed that all the N-doped TiO_2 photocatalysts were anatase phase with enhanced visible light absorption, narrow bandgap (2.64–2.50 eV), and small particle sizes ranging from 23.12–25.17 nm. The surface area decreased from 252.7 m^2/g to 72.3 m^2/g with an increased N:Ti molar ratio. The N:Ti molar ratio plays an important role in the formation of crystalline structure and surface area and performance. The photodegradation of HCHO vapor was the highest (70.59%) when the N:Ti molar ratio was 20:1. The best photodegradation efficiency was achieved using the N-doped TiO_2 calcined at 300°C for 1 h. This study signifies the importance of optimizing N:Ti molar ratio and calcination temperature for tuning the properties of the TiO_2 and the enhancing photodegradation of indoor HCHO vapor under visible light irradiation.

Keywords: *Photocatalytic oxidation, titanium dioxide, formaldehyde, visible light, nitrogen-doped, glycerol.*

INTRODUCTION

Indoor air pollution abatement is one of the major environmental challenges of the 21st century as a large population worldwide spends more than 65% of the time in the indoor environment [1]-[2]. The indoor air pollution due to formaldehyde (HCHO) can reach as high as 0.5 mg/L while its stipulated standard according to World Health Organization (WHO) is only 0.08 mg/L [3]. HCHO is considered as human carcinogen [4]-[5] and can cause sick building syndrome characterized by fatigue, skin and eye irritation, and headache. Complex and often expensive technologies have been investigated for indoor pollution abatement, especially for HCHO degradation [6]. However, the conventional treatment approaches such as adsorption, membrane filtration, and biological methods are unable to remove HCHO from the indoor environment.

Alternatively, photocatalytic technology based on various semiconductor oxides such CdS, CeO_2, Fe_2O_3, TiO_2, WO_3, ZnO, and ZnS has been widely investigated for decontaminating indoor air [7],[10]. Despite

overwhelming evidence of their performance, semiconductors oxides have yet to be employed on a large scale. Amongst the semiconductor oxides, TiO_2 based materials have shown great promise as low-cost photocatalysts for the degradation of indoor air pollutants [11]. However, TiO_2 can only be activated by ultraviolet light. Besides, TiO_2 has inherent drawbacks, such as a higher recombination rate of charged species and low efficiency under visible light irradiation. In order to be employed for large-scale indoor air pollution abatement, the TiO_2 needs to harvest the energy from indoor lightings or solar radiations and to eliminate the need for the recovery or separation from the air streams [12]. Two-pronged approach is required to tune the electronic band structure of TiO_2 and immobilize it on some inert medium such as glass which will help expand the capability of TiO_2 for degradation of HCHO and make the indoor air purification process more sustainable and accessible to all.

Over the years, various approaches have been adopted to improve the visible light photocatalytic activity of TiO_2 by implanting metal and nonmetals into its matrix, tuning the bandgap by inducing the structural or surface defects, and sensitization with dyes. Among these approaches, doping with N is believed to extend the light response of TiO_2 into the visible region, prevent charge species recombination and impart stability to the TiO_2 photocatalyst [13]. Despite the enhanced photocatalytic activity of N-doped TiO_2 for various indoor air pollutants' degradation [8],[14], its application for the photodegradation of HCHO is comparatively rare in the literature. Various approaches have also been explored for overcoming the problems of recovery or separation of the TiO_2 particles from waste streams. For instance, TiO_2 has been embedded into polyester fibres and its efficacy has been investigated for the degradation of HCHO from water [15]. The TiO_2 embedded fabrics have shown promising results. However, the studies regarding the use of immobilized TiO_2 to degrade HCHO vapor are rarely reported in the literature.

The present study aims to develop a photocatalytic system driven by visible light for the degradation of HCHO vapor from the indoor environment. For this purpose, the N-doped TiO_2 was synthesized via glycerol-assisted sol-gel technique followed by calcination at 300°C. The effect of various synthesis parameters, including nitrogen to titanium molar ratios, calcination temperature, and calcination duration, were investigated on the photocatalytic properties and performance of N-doped TiO_2 for HCHO degradation. The N-doped TiO_2 was immobilized on microscope glass sheets using the doctor blading method. The effect of the thickness in terms of TiO_2 loading was also investigated on the degradation of HCHO. The main idea is that the TiO_2 immobilized on the glass will derive the energy from the surrounding indoor environment. The presence of TiO_2 particles on the glass surface will trap air containing HCHO and allow the HCHO molecules to come into contact with TiO_2, resulting in its degradation. Though such studies have been carried out in various cities, for instance, in Paris, the TiO_2 coated glass was used in field experiments for the degradation of organic fractions including organic carbon, particulate matter, and inorganic soluble fractions [16], such studies are rare for indoor air pollutants degradation.

EXPERIMENTAL SECTION

Synthesis of N-doped TiO_2

The N-doped TiO_2 photocatalysts with different N:Ti molar ratios were synthesized using a modified sol-gel technique [17]. The detailed synthesis conditions for N-doped TiO_2 are shown in Table 1. Glycerol ($C_3H_8O_3$, 98%, Fischer Scientific) and deionized water were mixed in a fixed ratio of 9:1 (v/v). A specific amount of urea (CH_4N_2O, 99%, Merck) was dissolved in the aqueous glycerol solution to obtain a different molar concentration of N. Then, 0.1 mol of titanium tetrachloride ($TiCl_4$, 99%, Merck) was slowly added dropwise to the mixture under constant stirring to perform hydrolysis. Afterward, 300 mL of 2.5 M ammonia (NH_4OH, 25%, Merck) was added dropwise to the solution to raise to pH 10 for maximum precipitation. The sol was aged in the air for 24 h under continuous stirring to allow for further hydrolysis. Subsequently, the sol was dried for 24 h in an oven at 70°C and then calcined at different calcination temperatures and duration with a heating rate of 5°C min^{-1}. TiO_2 photocatalyst was synthesized using the same procedure without the addition of urea and calcined at 300°C for 1 h. The prepared samples were labelled as N-x-T, where 'x' and 'T' represents the N:Ti molar ratio (x = 0:1, 1:1, 5:1, 10:1, 15:1, 20:1, 25:1) and

Table 1 Synthesis conditions and nomenclature of the N-TiO_2 photocatalysts

Sample	N:Ti (molar)	Calcination temperature (°)	Calcination duration (h)
N-0:1-300	0:1	300	1
N-1:1-300	1:1	300	1
N-5:1-300	5:1	300	1
N-10:1-300	10:1	300	1
N-15:1-300	15:1	300	1
N-20:1-300	20:1	300	1
N-25:1-300	25:1	300	1
N-20:1-300 (2h)	20:1	300	2
N-20:1-300 (3h)	20:1	300	3
N-20:1-400	20:1	400	1
N-20:1-500	20:1	500	1

T denotes the calcination temperature (T = 300, 400, 500°C), respectively.

Characterization of the synthesized materials

The synthesized materials' crystalline structure, phase composition, and crystallite size were obtained using an X-ray diffractometer (PANalytical X'Pert^3 Powder) with *Cu Kα* radiation (40 kV, 40 mA). The scanning was carried out at 2θ angle between 5°–80° with a scan step size of 0.026261°. The average crystallite sizes of the prepared materials were calculated using Scherrer's formula from the characteristic diffraction peaks (101) plane of anatase TiO_2 at 2θ = 25° as given by:

$$D = \frac{K\lambda}{\beta \operatorname{Cos} \theta} \quad (1)$$

where, D is the average crystallite size (nm), K is the Scherrer's constant (0.9), λ is the X-ray wavelength (0.15418 nm), β is the full width at half maximum (FWHM) of the selected diffraction peak in radian and θ is the diffraction angle.

XPS data was collected via Thermo-Fisher Scientific spectrometer with C1s correction at 284.6 eV for calibration and Al Kα (1486.60 eV) as an x-ray excitation source. The instrument base pressure was 8×10^{-10} Torr. The high-resolution XPS spectra were acquired for a total of 8 min and 22.5 s using an analysis area of 300–700 μm with a 50.0 eV pass energy and an energy step size of 0.100 eV. The peaks were fitted using Gaussian curve fitting. Field emission scanning electron microscopy (FESEM) was used to examine the surface morphology of the synthesized materials. The FESEM images were captured at 10 kX magnification using the Carl Zeiss instrument (SUPRA 55VP) at an acceleration voltage of 30 kV. The diffuse reflectance UV-Visible (DRUV-Vis) spectrum of the sample was obtained in the UV-Visible region (λ = 200-800 nm) with a spectrometer (Agilent Carry100, Santa Clara, CA, USA). The physio-sorption isotherms of the samples were acquired at –195.8°C using Micromeritics ASAP 2020 analyzer (Micromeritcs Corps., Norcross, GA, USA). Before measurements, the samples were degassed at 300°C for 240 min to remove the impurities and moisture from the sample's surface. The specific surface area of the sample was calculated based on Brunauer, Emmett and Teller's (BET) method from the adsorption measurement at a relative pressure ranging from 0.05 to 0.3. The pore size of the sample was calculated from desorption data using Barrett-Joyner-Halenda (BJH) method.

Coating of the synthesized materials on glass

A microscope glass slide with a dimension of 2.4 cm × 7.62 cm was used as a substrate for coating or immobilizing the synthesized N-doped TiO_2 samples. The glass slides were cleaned in 2-propanol before coating. The N-doped TiO_2 samples were dispersed in 2-propanol at various masses (0.025, 0.05, and 0.075 g) and ultrasonicated for 5 min to achieve a homogeneous suspension. The suspension was uniformly coated onto the glass slides and the process was repeated to form three thin layers.

Photodegradation tests of N-doped TiO_2

The photodegradation performance of N-doped TiO_2 for HCHO was conducted in a batch mode using a 250-mL quartz photoreactor under visible light irradiation. The schematic illustration of the experimental setup is given in Figure 1. The N-doped TiO_2 coated on a glass slide (3) was fixed inside the quartz photoreactor (2). In a tightly sealed stainless-steel tube containing 37% HCHO (1), 3.22 ppm of HCHO vapor was diffused into the quartz photoreactor (2) by opening V1 and V2 valves. After 30 min of equilibration in the dark, the quartz photoreactor was irradiated at a distance of 7 cm from the bottom with a 150 W halogen lamp as the

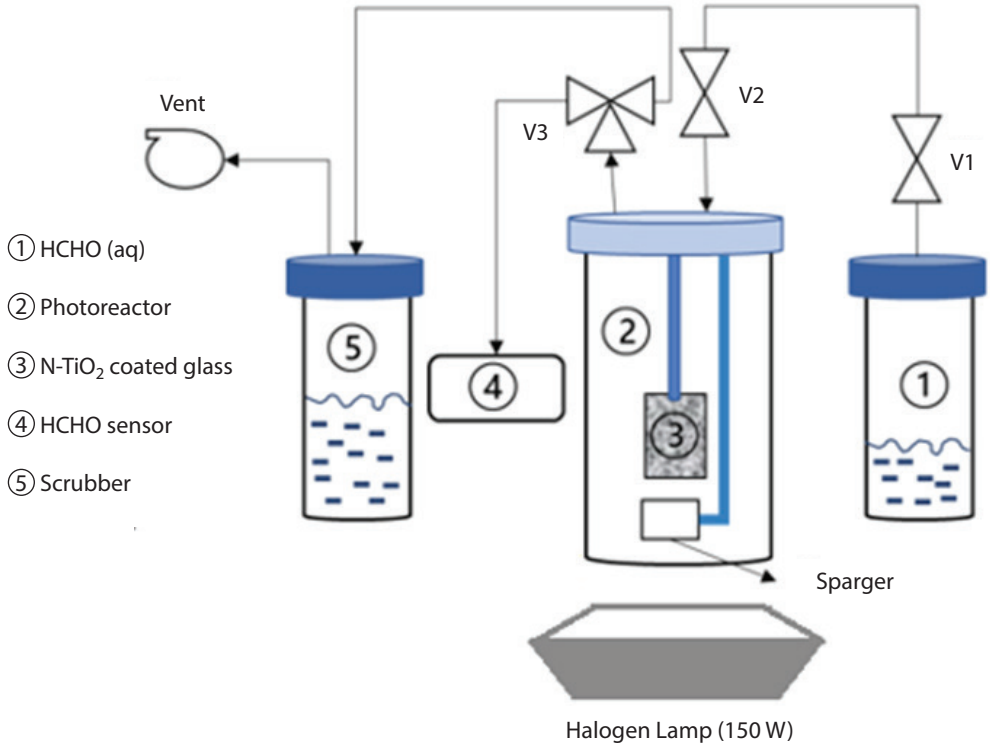

Figure 1 Schematic of the experimental setup used for photodegradation experiments

light source, which primarily consists of a visible light field. HCHO photodegradation was monitored using a HCHO sensor (4) by sampling at 10-min intervals for 30 min and 30-min intervals for another 120 min. After the reaction, the photoreactor was purged with He gas through the scrubber (5).

V3 was fitted with a wireless formaldehyde sensing meter to measure the HCHO vapor concentration. The sensor's operating range was up to 10 ppm. By using a cooling fan, the temperature of the photoreactor was held at 25±1°C during the photoreaction. The temperature monitoring of the photoreactor was carried out in a separate process having the same reaction conditions. The photodegradation of HCHO was determined using:

$$\text{HCHO}\ (\%) = \frac{\text{HCHO}_{initial} - \text{HCHO}_{time}}{\text{HCHO}_{initial}} \times 100\% \quad (2)$$

where HCHO (%) is the photodegradation efficiency, $\text{HCHO}_{initial}$ is the initial concentration of HCHO, which is 3.22 ppm, and HCHO_{time} is the concentration of HCHO at any given sampling interval.

RESULTS AND DISCUSSION

Properties of the N-doped TiO_2

The effect of various synthesis parameters, including N:Ti molar ratio, calcination temperature, and calcination duration, were investigated on the physicochemical properties of the N-doped TiO_2 photocatalysts, which are discussed in detail in the following sections.

Crystalline phase and morphology of N-doped TiO_2

XRD patterns of all the synthesized N-doped TiO_2 were analyzed to determine the effect of N:Ti molar ratio, calcination temperature and calcination duration on the crystalline structure. The XRD patterns as displayed in Figure 2a revealed that all the synthesized N-doped TiO_2 samples are anatase phase indicated by the presence of the characteristic peak at 2θ=25° matching well with the anatase plane (101) (JCPDS no. 21-1272) and in good agreement with previous studies [18].

It should be noted that the diffraction peaks of the N-25:1-300 become intense and sharper compared to the sample with lower N:Ti molar ratios, indicating that N:Ti molar ratio plays an important role in

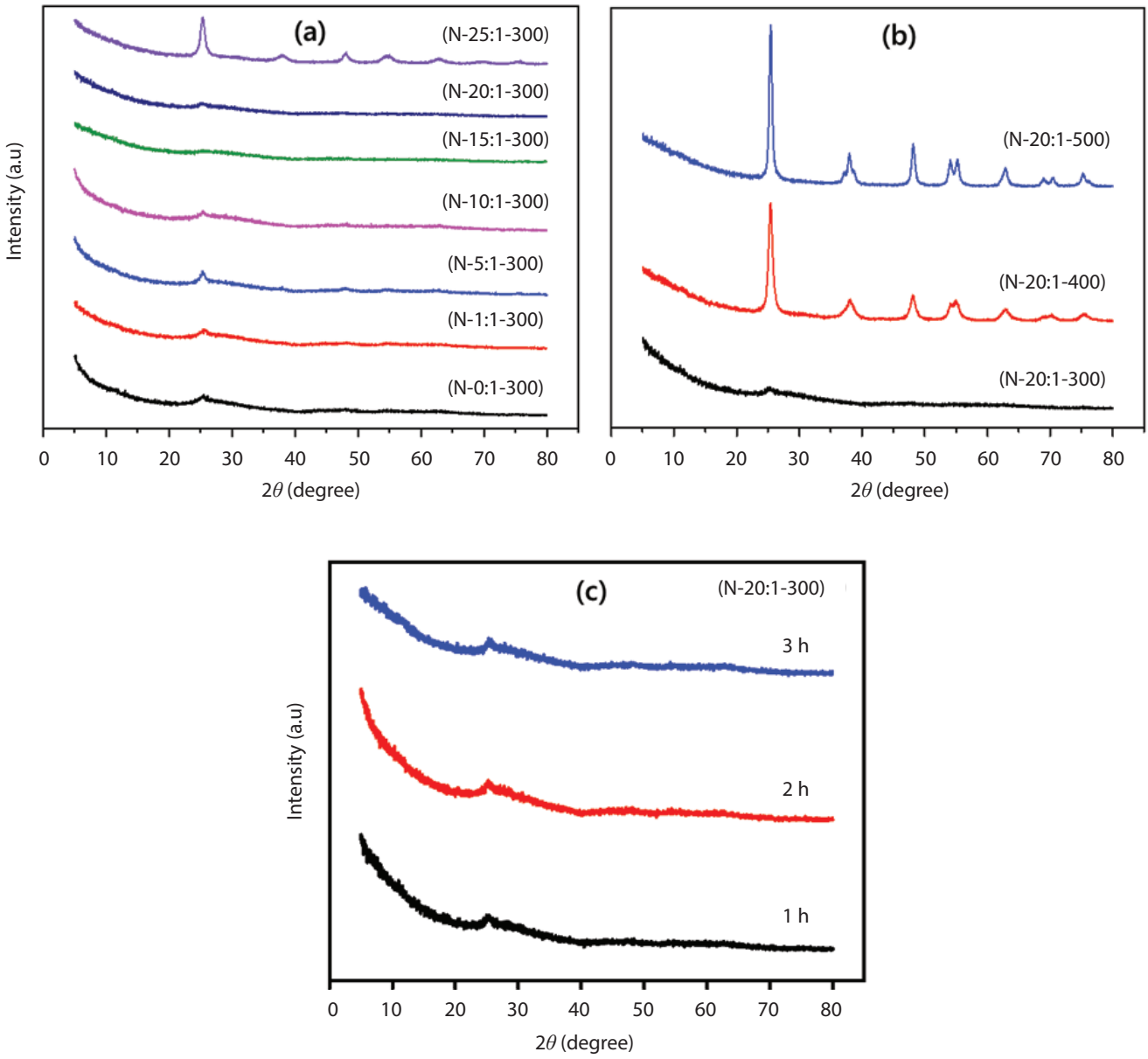

Figure 2 XRD patterns of the N-TiO_2 at different (a) N:Ti molar ratio, (b) calcination temperature (N:Ti=20:1), and (c) calcination duration (N:Ti=20:1)

the crystallization of the N-doped TiO_2. The other diffraction peak at 2θ=63° corresponding to (002) plane of rutile phase was not observed in the XRD pattern, which could appear during the crystallization of the N-TiO_2 [19]. This can be explained by the lower calcination temperature or the calcination in the oxygen atmosphere compared to the higher temperature and N_2 atmosphere in previous studies [18],[20]. Although the crystallinity of the N-doped TiO_2 samples decreased with decreasing N:Ti ratio, the (101) plane dominated the diffractogram.

Based on the preliminary results of photocatalytic activity, the sample N-20:1-300 showed enhanced performance and thus the effect of calcination temperature and calcination duration was investigated on the crystalline structure and phase composition of the sample. It was identified that the calcination temperature significantly affects the crystallinity of the N-doped TiO_2 as revealed by the XRD patterns shown in Figure 2b. The diffraction peak at 2θ=25° became sharper when the calcination temperature was increased to 400 and 500°C. On the other hand, the calcination duration did not significantly affect

either the crystalline phase or crystallinity of the samples. The average crystallite size increased from 8.53 nm to 28.45 nm with an increase in N:Ti molar ratio from 0:1 to 25:1. The average crystallite size of the N-20:1-300 also increased with increasing calcination temperature and calcination duration. Higher calcination temperatures or longer duration could cause the doped nitrogen to be desorbed or replaced by oxygen [21]. It can be concluded that the N:Ti molar ratio and calcination temperature play an important role in shaping the structure of the N-doped TiO_2 and, therefore must be given attention.

The FESEM images shown in Figure 3(a-c), revealed that the N-doped TiO_2 samples with an N:Ti ratio of 15:1, 20:1 and 25:1 are nanosized particles with spherical shape. The results demonstrated that N:Ti molar ratio has no significant effect on the morphology of the TiO_2 photocatalyst. The particle size of the samples was estimated randomly from 200 particles using image J software. The particle size distribution was estimated using Gaussian line fitting and the results are shown in Figure 3(d-f). The average particle diameter was 25.17 nm at N:Ti molar ratio of 15:1, whereas it was decreased to 24.70 nm when the N:Ti molar ratio was raised to 25:1. It is important to note that the TiO_2 samples synthesized without the addition of urea did not show any N content from EDX, which confirmed that the N is only from urea rather than from ammonia.

Electronic and optical properties of N-doped TiO_2

The XPS analysis was carried out to obtain information on the chemical environment of the N-doped TiO_2 photocatalysts. The XPS fitting parameters are listed in Table 2. The Ti2p XPS spectra of the N-doped samples with N:Ti ratio of 15:1, 20:1 and 25:1 were investigated. The high resolution fitted Ti2p XPS spectra of the samples are shown in Figure 4 (a-c). The deconvoluted Ti2p spectra of N-15-300 are shown in Figure 4a. Two symmetrical orbital doublets peaks located at binding energy (BE) 459.79 and 465.45 eV corresponded to $Ti2p_{3/2}$ and $Ti2p_{1/2}$, respectively [21–23]. The $Ti2p_{3/2}$ and $Ti2p_{1/2}$ peaks of the N-20:1-300 were situated slightly lower at BE of 459.35 and 465.03 eV, respectively, as displayed in Figure 4b. As the N:Ti molar ratio increased, the Ti2p peaks of N-25:1-300 shifted to higher BE of 460.79 and 466.55 eV (Figure 4c). The shift to lower BE may be attributed to the greater electronegativity of oxygen compared

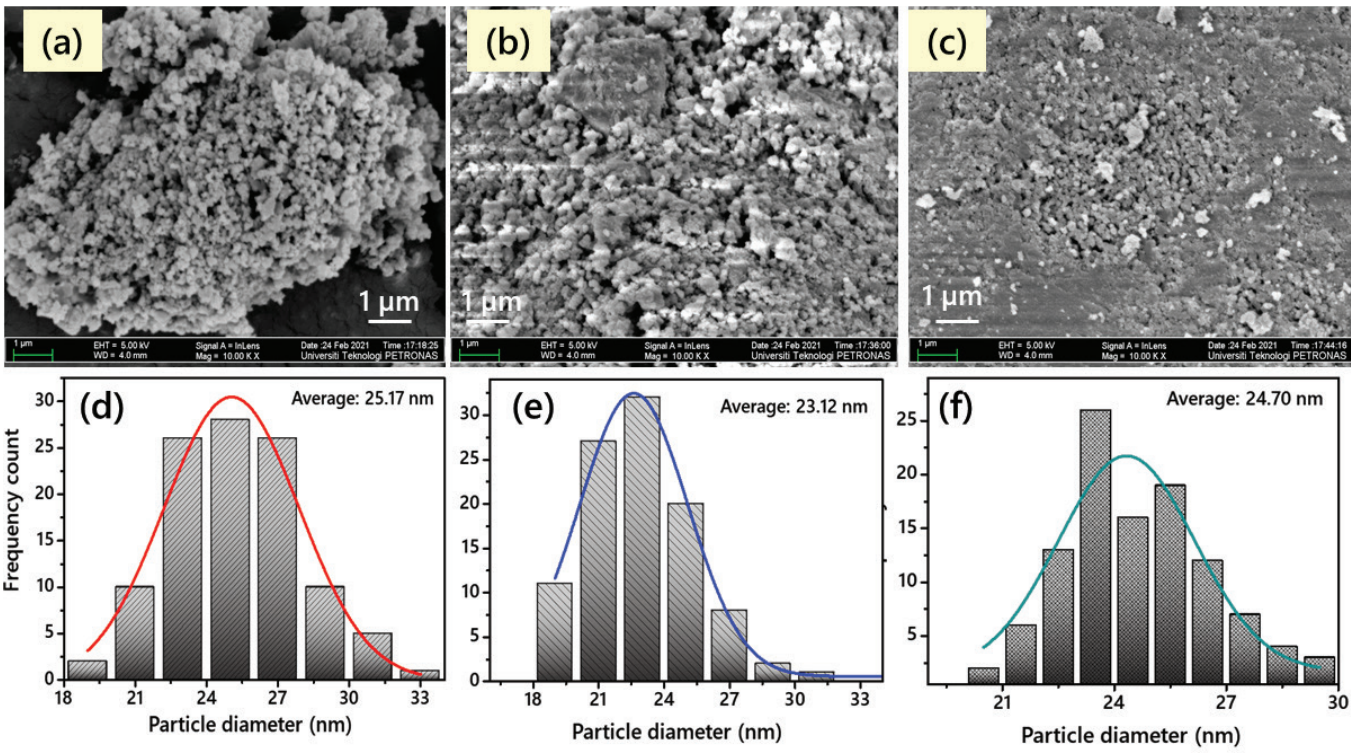

Figure 3 FESEM images of (a) N-15:1-300, (b) N-20:1-300, and (c) N-25:1-300, and particles size distribution of (d) N-15:1-300, (e) N-20:1-300, and (f) N-25:1-300 at 10 kX magnification

Table 2 XPS fitting parameters for N-TiO_2

Sample	$Ti2p_{3/2}$ (eV)	$Ti2p_{1/2}$ (eV)	N1s (eV)	O1s (eV)
N-15:1-300	459.79	465.45	400.57	531.13
N-20:1-300	459.35	465.03	401.74	532.23
N-25:1-300	460.79	466.55	402.18	532.83

to nitrogen, which increases the electron cloud density in the vicinity of Ti^{4+}, resulting in the change in the chemical environment of the Ti after N-doping [18].

The high-resolution deconvoluted O1s spectra of the N-doped TiO_2 samples are presented in Figure 4d-4f. Figure 4d shows the deconvoluted O1s spectra of the N-15:1-300. The spectra displayed two peaks at BE of 531.13 and 532.53 eV, which are assigned to BE values of lattice oxygen (Ti–O) and the Oxygen Vacancies (OVs), respectively [25]. The characteristic BE values of OVs were also present in the other N-doped samples with a higher N:Ti molar ratio of 20:1 and 25:1, suggesting that the OVs were created in the synthesized N-doped TiO_2 samples. However, the OVs BE values for N-20:1-300 (Figure 4e) and N-25:1-300 (Figure 4f) were located at slightly higher BE (532.23 and 532.83, respectively) compared to for N-15:1-300. As revealed by the peak areas, the OVs concentration was higher for samples with a lower N:Ti ratio (15:1 and 20:1) compared to 25:1. As shown in Figure 4f, the N-25:1-300 present an additional O1s peak at BE of 534.00 eV, which can be ascribed to the OH group present on the surface.

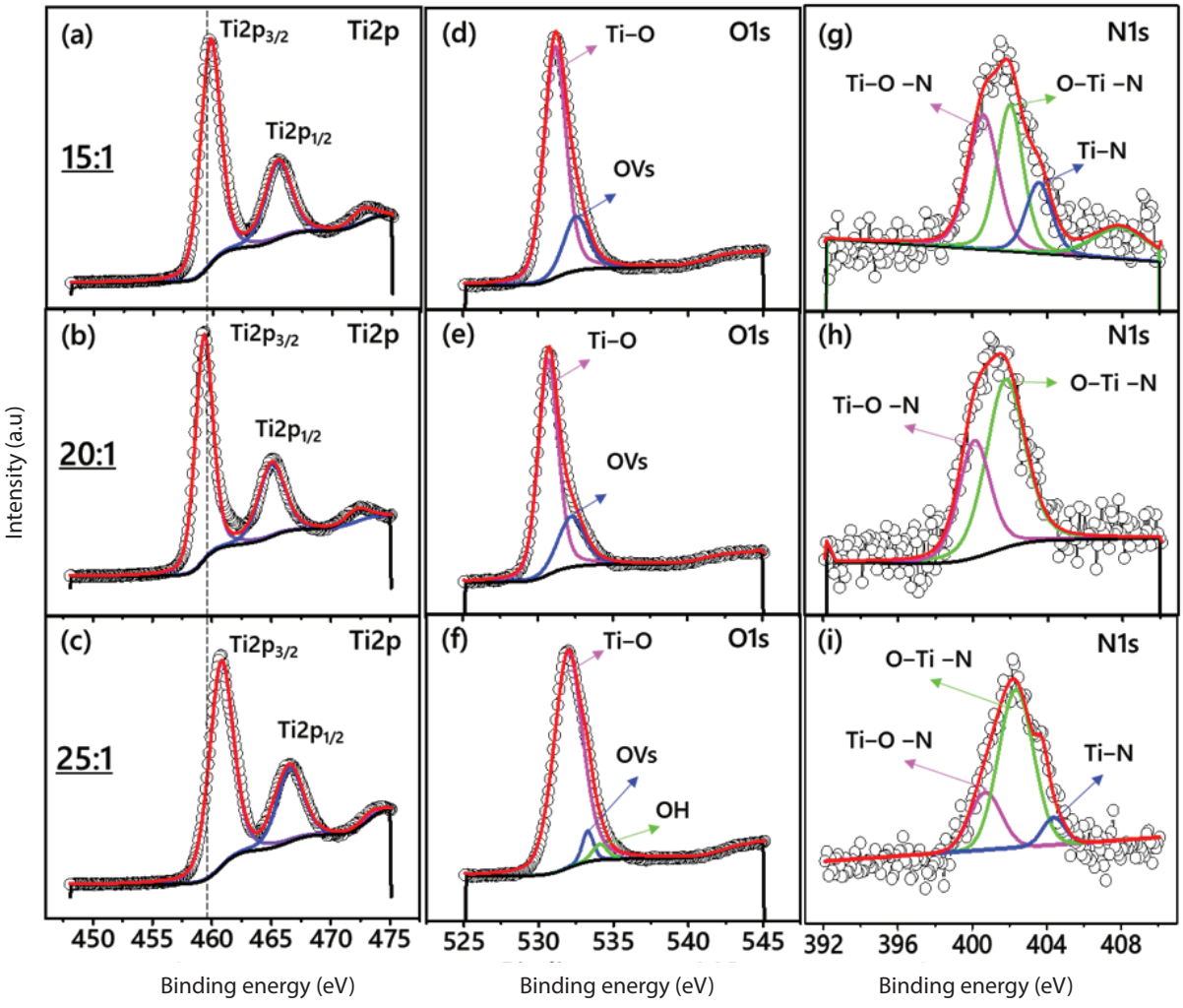

Figure 4 High resolution deconvoluted Ti2p XPS spectra (a) N-15:1-300, (b) N-20:1-300, and (c) N-25:1-300; O1s XPS spectra of (d) N-15:1-300, (e) N-20:1-300, and (f) N-25:1-300; and N1s XPS spectra of (g) N-15:1-300, (h) N-20:1-300, and (i) N-25:1-300

Generally, the presence of hydroxyl group facilitates the efficient separation of charge species (e^-/h^+) and improves the photocatalytic activity of the TiO_2 photocatalyst [26].

The deconvoluted N1s spectra of the N-doped TiO_2 is presented in Figure 4(g-i). The sample, N-15:1-300 showed the three peaks at 400.57, 402.00, and 403.55 eV which are associated with Ti-O-N, O-Ti-N, and Ti-N bonds linkages, respectively [27]. The sample N-20:1-300 showed two peaks at 401.74 and 400.08, whereas the BE value of the N Bond linkages was shifted to higher BE of 402.18 and 404.35 eV in N-25:1-300. The shift to higher BE can be explained on the basis of the evolution of OVs in N-doped TiO_2 sample. The increase in OVs favors decreasing interstitial doping than substitutional doping and the more the number of OVs, the more substitutional doping compared to interstitial [20].

The UV-vis spectra was recorded to determine the effect of N:Ti molar ratio on the optical absorbance and bandgap of TiO_2 photocatalyst. Figure 5a shows the absorbance spectra of the N-doped TiO_2 samples. It can be observed that the light absorption intensity was intensified with the increase in N:Ti molar ratio up to 20:1. However, further increase in N:Ti molar ratio to 25:1 does not significantly affect the light absorption property of the TiO_2 photocatalysts.

The bandgap of the N-doped TiO_2 samples were calculated using a Tauc plot, based on the relation $(ahv)^2 = k(hv\text{-}Eg)$, where hv is the energy of the incident light in eV, k a constant and α is the absorption coefficient relationship. The bandgap of the undoped TiO_2 was 2.96 eV [28] and it was monotonically decreased to 2.69, 2.50, and 2.61 eV with increasing N:Ti molar ratio to 15:1,20:1, 25:1. It can be seen that the bandgap shows significant reduction with increasing the N:Ti molar ratio which indicates that the bandgap of N-TiO_2 samples reduced due to the impurity level in the bandgap. The different N:Ti molar ratios may influence the absorption ability and photocatalytic activity of the N-doped TiO_2 under visible light irradiation. The low intensity of the Ti–O–N peaks in Figures 4g-4i suggest that the doped N ions do not accumulate on the surface of TiO_2 photocatalyst but are homogeneously distributed across the TiO_2 matrix.

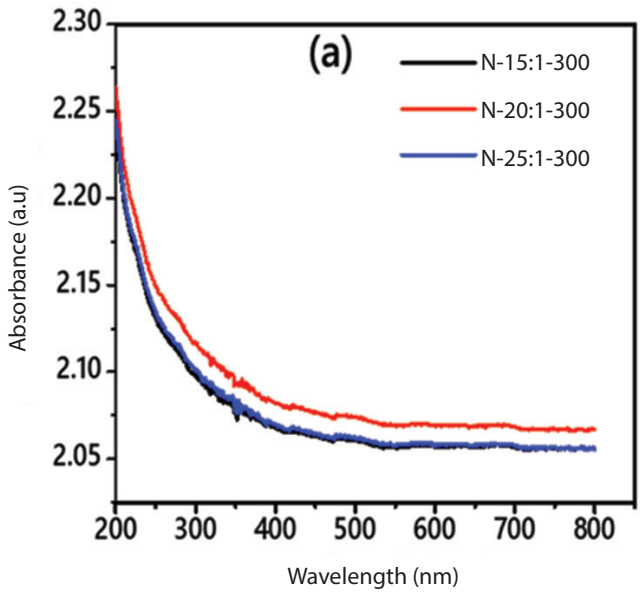

Figure 5 (a) UV-Vis absorption spectra of N-15:1-300, N-20:1-300, and N-25:1-300

Textural properties

The textural properties of the N-doped TiO_2 samples are summarized in Table 3. The nitrogen physisorption isotherms of the N-doped TiO_2 samples are shown in Figure 6. The desorption branch in the hysteresis loop is separated from the adsorption branch in the relative pressure (P/P) range of 0.4–0.9, 0.6–0.8, and 0.5–0.6 for N-15:1-300, N-20:1-300, and N-25:1-300, respectively. The isotherms of the N-15:1-300 and N-25:1-300 were characteristic of type IV isotherm and H2 hysteresis loop, indicating that the synthesized N-doped TiO_2 photocatalysts are mesoporous in nature. It should be noted that the isotherms of the N-20:1-300 are different from the two samples indicating the formation of cylindrical pores. The formation of pores with different morphology clearly demonstrates the role of a higher N:Ti molar ratio in engineering the pore structure, as titania is otherwise known to form ink-bottle type pores in the absence of structure directing agents [29].The isotherms also confirm their mesoporosity by the narrow pore size distribution ranging from 4.008–10.160 nm. The N-20:1-300 showed the highest specific surface area of 252.7 m^2/g. The other samples with lower and higher N:Ti molar ratios showed lower surface area. The decrease in surface area was observed with increasing dopant concentration which is consistent with the

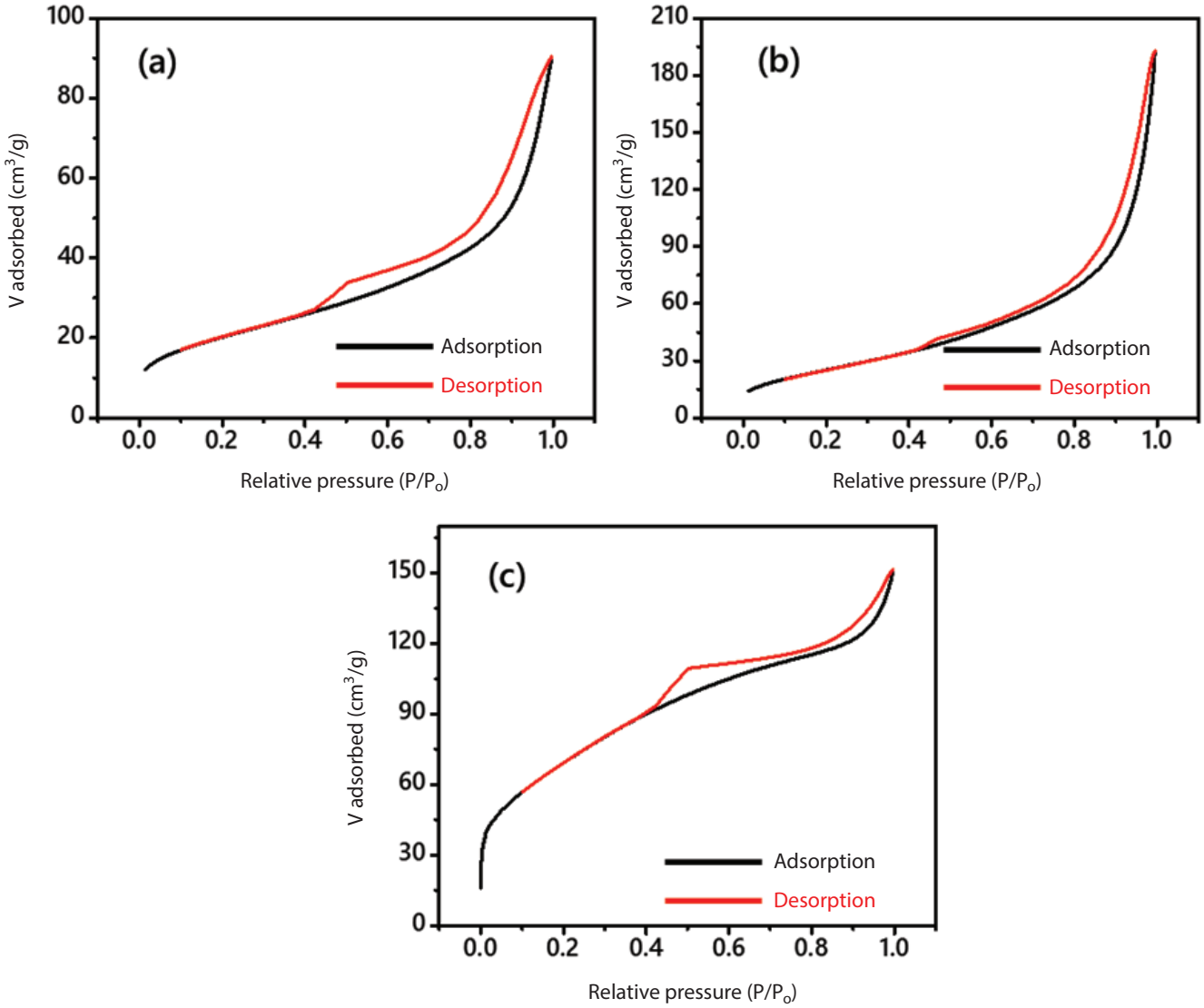

Figure 6 Nitrogen physisorption isotherms of (a) N-15:1-300, (b) N-20:1-300, and (c) N-25:1-300

previously reported study [21]. Commonly, high surface area and rich pore structure are favorable to supply more active centers and high adsorption capacity towards pollutant molecules resulting in better photocatalytic activity [30].

Table 3 BET surface area and pore parameters of N-doped TiO_2 powders at different N:Ti molar ratios

Sample	Specific Surface Area (m^2/g)	Pore Volume (cm^3/g)	Average Pore Size (nm)
N-15:1-300	93.7	0.301661	10.1601
N-20:1-300	252.7	0.229440	4.0088
N-25:1-300	72.3	0.144464	8.1829

Photodegradation of HCHO

The effect of N:Ti molar ratio, calcination temperature, calcination duration, and TiO_2 loading was evaluated on photodegradation of the HCHO vapor.

Effect of N:Ti molar ratio

The effect of N:Ti molar ratio was evaluated on the photodegradation of HCHO vapor under visible light irradiation. The normalized concentration of HCHO after 150 min of visible light irradiation is shown in Figure 7(a). The blank experiment shows that after introducing HCHO into the photoreactor for 150 min, the HCHO concentration drops by about 10%. The result showed that approximately 10% of the initial 3.22 ppm HCHO vapor was removed by the adsorption process of HCHO molecules on the surface of the

N-doped TiO_2 photocatalysts. The HCHO degradation efficiency was drastically enhanced when the visible light was introduced to the system from a 150 W halogen lamp. Among all the synthesized N-doped TiO_2 samples with different N:Ti molar ratio, the N-20:1-300 showed distinctly improved photodegradation of HCHO. About 57.09% of the HCHO was degraded within 60 min of visible light irradiation, suggesting faster degradation at the initial stage of the photoreaction. The HCHO degradation efficiency rose to 70.59% with extending the irradiation time 90 min. However, the HCHO degradation efficiency plateaued after 90 min suggesting the saturation of the photocatalysts surface. The reduced HCHO degradation efficiency later in the photoreaction may be due to HCHO molecules completely covering the TiO_2 surface, thereby preventing the active sites on the photocatalyst from further adsorption and subsequent degradation.The higher photodegradation ability of N-20:1-300 can be due to its higher surface area compared to the other samples and enhanced visible light absorption as well as lower bandgap. The localized N-doping states may have enabled N-doped TiO_2 to absorb visible light efficiently which leads to improved electron-hole pair separation [13]. The other N:Ti molar ratios also improved the HCHO degradation but not so large compared to 20:1. N-15:1-300 could degrade only 13.36% of HCHO after 60 min of visible light irradiation and the degradation efficiency rose to 43.25% after 150 min of reaction time.

On the other hand, N-25:1-300 achieved 55.02% HCHO removal efficiency after 150 min of visible light irradiation which is 1.28-fold less than the N-doped TiO_2 sample with N:Ti molar ratio of 20:1. The results demonstrated that a specific N:Ti molar ratio makes N-doped TiO_2 to effectively degrade HCHO vapor. In the present case, the N:Ti molar ratio of 20:1 was the most promising for enhancing the photodegradation of HCHO vapor under visible light irradiation.

Effect of calcination temperature

The best performing N-doped TiO_2 sample (20:1) was further treated at different calcination temperatures, including 300, 400, and 500°C to investigate the effect of calcination temperature on photodegradation of HCHO vapor. The normalized concentration of HCHO after 150 min of visible light irradiation is shown in Figure 7(b).

It was found that the N-doped TiO_2 sample with 20:1 of N:Ti molar ratio and calcined at 300°C is the most effective for photodegradation of HCHO under visible irradiation suggested by its higher efficiency of 70.59% compared to 44.29 and 43.94% by the N-doped TiO_2 samples calcined at 400 and 500°C, respectively. This occurrence might be due to the lower photon absorption efficiency at higher calcination temperatures that are influenced by the agglomeration and sintering process that occur on the photocatalyst's surface during the heat treatment process, resulting in lower specific surface area of the N-doped TiO_2 photocatalyst. Furthermore, increasing calcination temperature results in loss of nitrogen content and subsequently increased the bandgap of the photocatalyst [31]. In contrast, previous studies have reported that the photodegradation of HCHO increases with the increasing calcination temperature of the anodized TiO_2 nanotubes [32]. The discrepancy in the results compared to previous studies could be attributed to the basic morphological features as previous studies have investigated the effect of calcination temperature on HCHO using nanotubes, whereas the current study used the TiO_2 particles.

It is very important to note that the most convenient temperature of 300°C gives the best results in HCHO degradation as opposed to the previous work, which reported that the best performing TiO_2 photocatalyst was calcined at 450°C. The lower calcination temperature is beneficial because it can reduce the energy consumption while fabricating N-doped TiO_2 photocatalyst for photodegradation of HCHO vapor. The photodegradation efficiency of HCHO (70.59%) under visible light by the N-doped TiO_2 sample with N:Ti molar ratio of 20:1 and calcination temperature of 300°C is higher among the synthesized samples.

Effect of calcination duration

Since the N-20:1-300 sample has shown the best performance for photodegradation of HCHO vapor, therefore this sample was further calcined at 300°C for a different duration to investigate the effect of calcination duration on photodegradation of HCHO under visible light irradiation. The normalized concentration of HCHO after 150 min of visible light irradiation is displayed in Figure 7(c). It can be observed that increasing the calcination duration worse off the

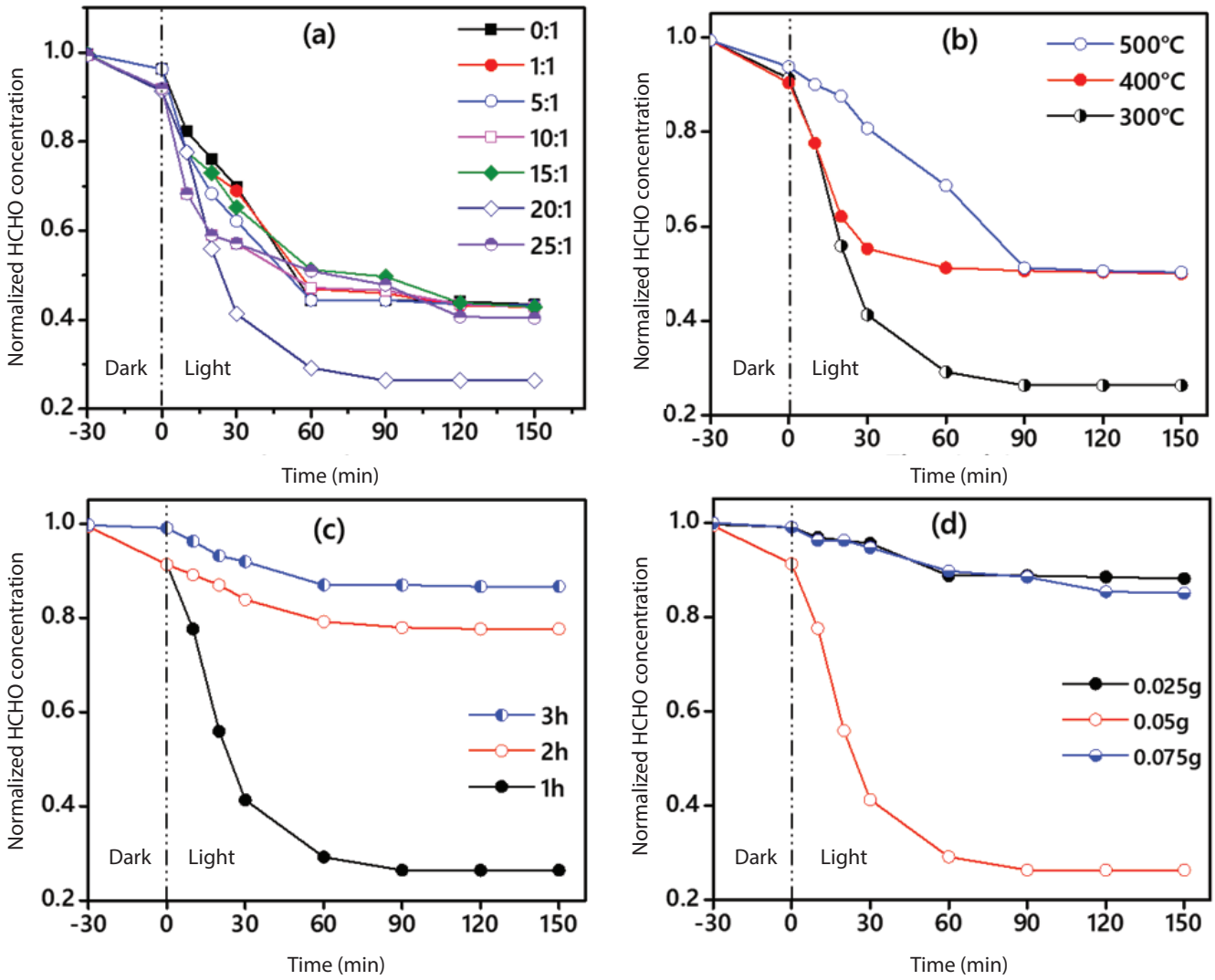

Figure 7 (a) Effect of N:Ti molar ratio, (b) effect of calcination temperature, (c) effect of calcination duration, and (d) effect of N-20:1-300 loading on photodegradation of HCHO

photodegradation of HCHO by N-doped TiO_2. The photodegradation of HCHO drops from 70.59% to only 13.49% and 3.46% by increasing calcination duration from 1 h to 2 h and 3 h, respectively. The increase in calcination duration might have decreased the specific surface area which is revealed by previous studies [33]. The lower photodegradation efficiency (59.7%) of HCHO by N-doped samples calcined at 600°C for 1.5 h was also reported by [34]. The results demonstrated that the calcination duration has a significant effect on the photodegradation efficiency of HCHO vapor, where the lower calcination duration results in better photodegradation of HCHO vapor and the higher calcination duration reduces the photodegradation efficiency of HCHO vapor under visible light irradiation.

Effect of TiO_2 loading

Different amounts including 0.025, 0.05, and 0.075 g of N-doped TiO_2 were coated on the glass slides for the purpose to investigate the effect of photocatalyst loading on photodegradation efficiency of HCHO vapor. The results of different photocatalyst loading are presented in Figure 7(d). The N-doped TiO_2 loading of 0.05 g on glass slides showed the best photodegradation efficiency (70.59%) of HCHO under 90 min of visible light irradiation. On the other hand, the TiO_2 loading of 0.025 and 0.075 g of N-doped TiO_2 on the glass slide were able only to degrade less than 10% of the HCHO vapor. The results demonstrate that 0.05 g of N-doped TiO_2 loading on the glass slide is favorable for enhanced photodegradation of HCHO under visible light irradiation. This can be due to

the decrease in the number of photons to strike on the surface of TiO_2 due to light attenuation and/or scattering by solid nanoparticles [35].

Mechanism of photodegradation of HCHO by N-doped TiO_2

The mechanism of photodegradation of HCHO vapor by N-doped TiO_2 under visible light irradiation can be explained based on the results obtained in the present study and previous literature. Generally, photocatalytic degradation of gaseous pollutants mainly includes two steps which are gas adsorption on the surface of the photocatalyst and photodegradation. After the gaseous pollutant as adsorbed on the photocatalyst surface, a certain amount of the adsorbed molecules were degraded by photocatalytic degradation [36] the Langmuir-Hinshelwood (L-H).

In the presence of light, photocatalytic degradation of HCHO occurs on TiO_2 surface and the mechanism can be explained using the following basic steps as shown in Equations 3 to 11 [31-32]:

I. Light absorption that leads to the formation of $e^-_{CB} + h^+_{VB}$ pairs:

$$TiO_2 + hv \rightarrow e^-_{CB} + h^+_{VB} \quad (3)$$

II. When the charge carriers of e^-_{CB} and h^+_{VB} recombined, a photoreaction occurred and resulting in the formation of heat:

$$e^-_{CB} + h^+_{VB} \rightarrow TiO_2 + \text{heat} \quad (4)$$

III. The adsorption of water and oxygen on the surface of TiO_2 produced radicals:

$$h^+ + H_2O_{(ads)} \rightarrow {}^{\bullet}OH + H^+ \quad (5)$$

$$O_{2(ads)} + e^-_{CB} \rightarrow {}^{\bullet}O_2^-{}_{,ads} \quad (6)$$

IV. The potential mechanism for photodegradation of HCHO progressed through the following steps as follows:

$$HCHO + {}^{\bullet}OH \rightarrow {}^{\bullet}CHO + H_2O \quad (7)$$

$$^{\bullet}CHO + \bullet OH \rightarrow HCOOH \quad (8)$$

$$^{\bullet}CHO + \bullet O_2^-{}_{,ads} \rightarrow HCO_3^- (H^+) \rightarrow HCOOOH (+HCHO) \rightarrow HCOOH \quad (9)$$

$$HCOOH (-H+) \rightarrow HCOO^- (+\bullet OH) \rightarrow H_2O + \bullet CO_2^- \text{ or } HCOO^- (+h_{VB}+) \rightarrow H^+ + \bullet CO_2^- \quad (10)$$

$$^{\bullet}CO_2^- ([O], \bullet OH, h^+) \rightarrow CO_2 \quad (11)$$

According to [39], the HCHO mechanism for degradation can be described as follows. As shown in Equation 3, when TiO_2 was illuminated with photons with an energy greater than its bandgap, the electrons and holes were formed simultaneously in the conduction band and valence band, respectively. The oxygen adsorbed on the surface of TiO_2 was reduced to $^{\bullet}O_2^-$ by the photoelectrons on the surface, and trace water was degraded to •OH by the valence band holes. The degradation of HCHO proceeded with the produced $^{\bullet}O_2^-$ or •OH, either way will lead to the degradation of HCHO. The $^{\bullet}O_2^-$ or •OH radicals further attacked the C–H bonds in HCHO and then reacted with the liberated hydrogen atoms to form new free radicals, propagating a chain reaction. The initial stage of the degradation process resulted in the formation of formic acid and ultimately mineralization of HCHO molecules into H_2O and CO_2.

CONCLUSION

N-doped TiO_2 photocatalyst was successfully synthesized by a simple sol-gel technique using glycerol and water as the reaction medium and urea as N-precursor. The as-synthesized N-doped TiO_2 samples were transformed into anatase phase by calcining at 300°C and 1h duration. The N-doped TiO_2 with N:Ti molar ratio of 20:1 was determined to be the best photocatalyst demonstrating 70.59% photodegradation of HCHO vapor under visible light irradiation. The enhanced photocatalytic performance can be attributed to the improved visible light absorption, the lower bandgap of 2.50 eV, and the higher surface area of 252.7 m^2/g. The calcination temperature of 300°C and duration of 1 h were the most appropriate for enhancing photodegradation of HCHO, while the higher calcination temperature of 400 and 500°C led to declined photodegradation efficiency of HCHO vapor under visible light irradiation. It can be concluded that the doping TiO_2 with N significantly improves the photocatalytic properties and photocatalytic degradation of gaseous formaldehyde under visible light irradiation. The future work will be focused on

investigating the molar ratio of N:Ti between 15:1 and 25:1, lower calcination temperature and duration on the properties and performance of N-TiO_2 for the removal of formaldehyde.

ACKNOWLEDGMENT

The author would like to thank the Centre of Research in Ionic Liquids (CORIL), Centre of Innovative Nanostructures and Nanodevices (COINN) and Photocatalyst Laboratory at Catalyst Research (CARE) Laboratory in Universiti Teknologi PETRONAS for providing the facilities, financial support from the Ministry of Higher Education Malaysia (FRGS/1/2016/STG01/UTP/02/1), from Yayasan Universiti Teknologi PETRONAS (YUTP 015L0-276), Malaysia and UTM-UTP CRG (015MC0-019), Malaysia are greatly acknowledged.

REFERENCES

[1] X. He et al., "Winter vacation, indoor air pollution and respiratory health among rural college students: A case study in Gansu Province, China," *Building and Environment*, 188, p. 107481, 2021.

[2] E. Cooper, Y. Wang, S. Stamp, E. Burman, & D. Mumovic, "Use of portable air purifiers in homes: Operating behaviour, effect on indoor PM2.5 and perceived indoor air quality," *Building and Environment*, 191, p. 107621, 2021.

[3] E. J. Herrera-López et al., "A control approach to regulate formaldehyde concentrations indoors a gross anatomy laboratory via a switched fuzzy logic system," *Building and Environment*, 188, p. 107492, 2021.

[4] J. K. McLaughlin, "Formaldehyde and cancer: a critical review," *International Archive Occupational Environmental Health*, 66, 5, pp. 295–301, 1994.

[5] G. D. Nielsen & P. Wolkoff, "Cancer effects of formaldehyde: a proposal for an indoor air guideline value," *Archive Toxicology*, 84, 6, pp. 423, 2010.

[6] N. Lu, J. Pei, Y. Zhao, R. Qi, & J. Liu, "Performance of a biological degradation method for indoor formaldehyde removal," *Building Environmental*, 57, pp. 253, 2012.

[7] W. Liang, J. Li, & Y. Jin, "Photo-catalytic degradation of gaseous formaldehyde by TiO_2/UV, Ag/TiO_2/UV and Ce/TiO_2/UV," *Building and Environmental*, 51, pp. 345, 2012.

[8] X. Hu, C. Li, Z. Sun, J. Song, & S. Zheng, "Enhanced photocatalytic removal of indoor formaldehyde by ternary heterogeneous BiOCl/TiO_2/sepiolite composite under solar and visible light," *Building Enviromental.*, 168, p. 106481, 2020.

[9] J. Pei, X. Han, & Y. Lu, "Performance and kinetics of catalytic oxidation of formaldehyde over copper manganese oxide catalyst," *Building and Environmental*, 84, p. 134, 2015.

[10] E. I. Cedillo-González, R. Riccò, M. Montorsi, M. Montorsi, P. Falcaro, & C. Siligardi, "Self-cleaning glass prepared from a commercial TiO_2 nano-dispersion and its photocatalytic performance under common anthropogenic and atmospheric factors," *Building and Environmental*, 71, p. 7, 2014.

[11] A. H. Mamaghani, F. Haghighat, & C. S. Lee, "Effect of titanium dioxide properties and support material on photocatalytic oxidation of indoor air pollutants," *Building and Environmental*, 189, p. 107518, 2021.

[12] H. Dong et al., "An overview on limitations of TiO_2-based particles for photocatalytic degradation of organic pollutants and the corresponding countermeasures," *Water Resource*, 79, p. 128, 2015.

[13] P. H. Le et al., "Enhanced photocatalytic performance of nitrogen-doped TiO_2 nanotube arrays using a simple annealing process," *Micromachines*, 9, 12, p.12, 2018.

[14] M. Z. Guo & C. S. Poon, "Photocatalytic NO removal of concrete surface layers intermixed with TiO_2," *Building and Environmental*, 70, p. 102, 2013.

[15] Xu et al., "Colored TiO_2 composites embedded on fabrics as photocatalysts: Decontamination of formaldehyde and deactivation of bacteria in water and air," *Chemical Engineering Journal*, 375, p. 121949, 2019.

[16] Chabas et al., "Behaviour of self-cleaning glass in urban atmosphere," *Building and Environmental*, 43, 12, p. 2124, 2008.

[17] X. Cheng, X. Yu, Z. Xing, & L. Yang, "Synthesis and characterization of N-doped TiO_2 and its enhanced visible-light photocatalytic activity," *Arabian Journal of Chemistry*, 9, pp. S1706, 2016.

[18] J. Huang, L. Dou, J. Li, J. Zhong, M. Li, & T. Wang, "Excellent visible light responsive photocatalytic behavior of N-doped TiO_2 toward decontamination of organic pollutants," *Journal of Hazardous Materials*, 403, p. 123857, 2021,

[19] A. Panepinto, J. Dervaux, P. A. Cormier, M. Boujtita, F. Odobel, & R. Snyders, "Synthesis of p-type N-doped TiO_2 thin films by co-reactive magnetron sputtering," *Plasma Processes and Polymers*, 17, 3, p. 1900203, 2020.

[20] A. Panepinto, D. Cossement, & R. Snyders, "Experimental and theoretical study of the synthesis of N-doped TiO_2 by N ion implantation of TiO_2 thin films," *Applied Surface Science*, 541, p. 148493, 2021.

[21] Y. Y. Gurkan, N. Turkten, A. Hatipoglu, & Z. Cinar, "Photocatalytic degradation of cefazolin over N-doped TiO_2 under UV and sunlight irradiation: Prediction of the reaction paths via conceptual DFT," *Chemical Engineering Journal,* 184, pp. 113, 2012.

[22] A. Panepinto, D. Cornil, P. Guttmann, C. Bittencourt, J. Cornil, & R. Snyders, "Fine control of the chemistry of nitrogen doping in TiO_2: A joint experimental and theoretical study," *Journal of Physical Chemistry C*, 124, 31, pp. 17401, 2020.

[23] B. Bharti, S. Kumar, H. N. Lee, & R. Kumar, "Formation of oxygen vacancies and Ti^{3+} state in TiO_2 thin film and enhanced optical properties by air plasma treatment," *Scientific Reports*, 6, p. 32355, 2016.

[24] M. C. Biesinger, B. P. Payne, A. P. Grosvenor, L. W. M. Lau, A. R. Gerson, & R. St. C. Smart, "Resolving surface chemical states in XPS analysis of first row transition metals, oxides and hydroxides: Cr, Mn, Fe, Co and Ni," *Applied Surface Science*, 257, 7, pp. 2717, 2011.

[25] B. Zhao, X. Wang, Y. Zhang, J. Gao, Z. Chen, & Z. Lu, "Synergism of oxygen vacancies, Ti^{3+} and N dopants on the visible-light photocatalytic activity of N-doped TiO_2," *Journal of Photochemistry and Photobiology A: Chemistry*, 382, p. 111928, 2019.

[26] Huang et al., "Ionic liquid assisted hydrothermal preparation of TiO_2 with largely enhanced photocatalytic performance originated from effective separation of photoinduced carriers," *Journal of Physical Chemistry of Solids*, 139, p. 109323, 2020.

[27] D. A. Agyeman, K. Song, S. H. Kang, M. R. Jo, E. Cho, & Y. M. Kang, "An improved catalytic effect of nitrogen-doped TiO_2 nanofibers for rechargeable $Li–O_2$ batteries; the role of oxidation states and vacancies on the surface," *Journal of Material Chemistry. A*, 3, 45, pp. 22557, 2015.

[28] R. Nawaz, C. F. Kait, H. Y. Chia, M. H. Isa, & L. W. Huei, "Glycerol-mediated facile synthesis of colored titania nanoparticles for visible light photodegradation of phenolic compounds," *Nanomaterials*, 9, 11, 2019.

[29] T.Z. Ren, Z. Y. Yuan, & B. L. Su, "Surfactant-assisted preparation of hollow microspheres of mesoporous TiO_2," *Chemical Physics Letters*, 374, 1, p. 170, 2003.

[30] D. Ma, J. Zhong, J. Li, C. Burda, & R. Duan, "Preparation and photocatalytic performance of MWCNTs/BiOCl: Evidence for the superoxide radical participation in the degradation mechanism of phenol," *Applied Surface Science*, 480, p. 395, 2019.

[31] Suwannaruang et al., "Influence of nitrogen content levels on structural properties and photocatalytic activities of nanorice-like N-doped TiO_2 with various calcination temperatures," *Materials Research Bulletin*, 105, pp. 265, 2018.

[32] N. T. Sahrin, R. Nawaz, C. Fai Kait, S. L. Lee, & M. D. H. Wirzal, "Visible light photodegradation of formaldehyde over TiO_2 nanotubes synthesized via electrochemical anodization of titanium foil," *Nanomaterials*, 10, 1, 2020.

[33] Y.T. Lin, C.H. Weng, H.J. Hsu, Y.H. Lin, & C.C. Shiesh, "The synergistic effect of nitrogen dopant and calcination temperature on the visible-light-induced photoactivity of N-doped TiO_2," *International Journal of Photoenergy*, 2013, p. e268723,

[34] Wu et al., "High-performance and renewable supercapacitors based on TiO_2 nanotube array electrodes treated by an electrochemical doping approach," *Electrochimica Acta*, 116, pp. 129, 2014.

[34] X. Zhao, G. Zhang, & Z. Zhang, "TiO_2-based catalysts for photocatalytic reduction of aqueous oxyanions: State-of-the-art and future prospects," *Environment International*, 136, p. 105453, 2020.

[35] P. Sun, J. Zhang, W. Liu, Q. Wang, & W. Cao, "Modification to L-H kinetics model and its application in the

investigation on photodegradation of gaseous benzene by nitrogen-doped TiO_2," *Catalysts*, 8, 8, 2018.

[37] G. L. Chiarello, D. Ferri, & E. Selli, "Effect of the CH_3OH/H_2O ratio on the mechanism of the gas-phase photocatalytic reforming of methanol on noble metal-modified TiO_2," *Journal of Catalysis,* 280, 2, p. 168, 2011.

[38] J. Yang, D. Li, Z. Zhang, Q. Li, and H. Wang, "A study of the photocatalytic oxidation of formaldehyde on $Pt/Fe_2O_3/TiO_2$," *Journal of Photochemistry and Photobiology A: Chemistry*, 137, 2, pp. 197, 2000.

[39] D. Gu, B. Wang, Y. Zhu, and H. Wu, "Photocatalytic degradation of gaseous formaldehyde by modified hierarchical TiO_2 nanotubes at room temperature," *Australian Journal of Chemistry*, 69, 3, pp. 343, 2016.